Geochemistry, Geophysics, Geosystems

RESEARCH ARTICLE
10.1029/2018GC007730

Key Points:
- Low-velocity anomaly is imaged under Rungwe Volcanic Province and northern Malawi rift
- Low-velocity anomaly is attributed to upwelling of warm mantle around side of Bangweulu Craton lithosphere
- Lithosphere beneath the Malawi rift may have been weakened prior to rifting

Supporting Information:
- Supporting Information S1

Correspondence to:
A. A. Nyblade,
aan2@psu.edu

Citation:
Grijalva, A., Nyblade, A. A., Homman, K., Accardo, N. J., Gaherty, J. B., Ebinger, C. J., et al. (2018). Seismic evidence for plume- and craton-influenced upper mantle structure beneath the northern Malawi rift and the Rungwe Volcanic Province, East Africa. *Geochemistry, Geophysics, Geosystems*, *19*. https://doi.org/10.1029/2018GC007730

Received 19 JUN 2018
Accepted 25 SEP 2018
Accepted article online 28 SEP 2018

©2018. American Geophysical Union. All Rights Reserved.

Seismic Evidence for Plume- and Craton-Influenced Upper Mantle Structure Beneath the Northern Malawi Rift and the Rungwe Volcanic Province, East Africa

Ashley Grijalva[1], Andrew A. Nyblade[1,2], Kyle Homman[1], Natalie J. Accardo[3], James B. Gaherty[3], Cynthia J. Ebinger[4], Donna J. Shillington[3], Patrick R. N. Chindandali[5], Gabriel Mbogoni[6], Richard Wambura Ferdinand[7], Gabriel Mulibo[7], J. P. O'Donnell[1], Marsella Kachingwe[1], and Gabrielle Tepp[8]

[1]Department of Geosciences, The Pennsylvania State University, State College, PA, USA, [2]School of Geosciences, The University of the Witwatersrand, Johannesburg, South Africa, [3]Lamont-Doherty Earth Observatory of Columbia University, Palisades, NY, USA, [4]Department of Earth and Environmental Sciences, Tulane University of Louisiana, New Orleans, LA, USA, [5]Geological Survey of Malawi, Zomba, Malawi, [6]Geological Survey of Tanzania, Dodoma, Tanzania, [7]Geology Department, University of Dar es Salaam, Dar es Salaam, Tanzania, [8]Department of Physics and Astronomy, University of Rochester, Rochester, NY, USA

Abstract *P* and *S* wave tomographic models have been developed for the northern Malawi rift and adjacent Rungwe Volcanic Province (RVP) using data from the Study of Extension and maGmatism in Malawi aNd Tanzania project and data from previous networks in the study area. The main features of the models are a low-velocity zone (LVZ) with δVp = ~−1.5–2.0% and δVs = ~−2–3% centered beneath the RVP, a lower-amplitude LVZ (δVp = ~−1.0–1.3% and δVs = ~−0.7–1%) to the southeast of the RVP beneath the center and northeastern side of the northern Malawi rift, a shift of the lower-amplitude anomaly at ~−10° to −11° to the west beneath the central basin and to the western side of the rift, and a fast anomaly at all depths beneath the Bangweulu Craton. The LVZ widens further at depths >~150–200 km and extends to the north beneath northwestern Malawi, wrapping around the fast anomaly beneath the craton. We attribute the LVZ beneath the RVP and the northern Malawi rift to the flow of warm, superplume mantle from the southwest, upwelling beneath and around the Bangweulu Craton lithosphere, consistent with high $^3He/^4He$ values from the RVP. The LVZ under the RVP and northern Malawi rift strongly indicates that the rifted lithosphere has been thermally perturbed. Given that volcanism in the RVP began about 10 million years earlier than the rift faulting, thermal and/or magmatic weakening of the lithosphere may have begun prior to the onset of rifting.

Plain Language Summary *P* and *S* wave tomographic models have been developed for the northern Malawi rift and adjacent Rungwe Volcanic Province (RVP) using data from the Study of Extension and maGmatism in Malawi aNd Tanzania project and data from previous networks in the study area. A low-velocity anomaly is imaged under the RVP and northern Malawi rift. We attribute the low-velocity anomaly to flow of warm mantle from the African superplume to the southwest of the study area, which has migrated around the side of thick Bangweulu Craton lithosphere and upwelled beneath the thinner mobile belt lithosphere to the east of the Bangweulu Craton. The observation that volcanism began in the RVP prior to the onset of rifting suggests that the lithosphere beneath the Malawi rift may have been thermally weakened prior to rifting.

1. Introduction

An outstanding challenge in continental dynamics is understanding how strong continental lithosphere ruptures in the early stages of rifting (e.g., Buck, 2004, 2006). Continental rupture can be achieved with a modest amount of tectonic stress if a weakening mechanism is present, for example, magmatism and/or dike intrusions (e.g., Bialas et al., 2010) or widespread metasomatism (e.g., Foley & Fischer, 2017; Rooney et al., 2014; Rosenthal et al., 2009), but is difficult to achieve in the absence of a weakening mechanism. Analytical and numerical simulations of continental lithosphere (e.g., Bialas et al., 2010; Bott, 1991; Buck, 2004) and observational studies (e.g., Bastow & Keir, 2011; Kampunzu & Mohr, 1991; Morgan, 1971; Sengör & Burke, 1978; White & McKenzie, 1989) have suggested that magmatism and hydration from

upwelling mantle (metasomatism; e.g., Foley & Fischer, 2017; Rooney et al., 2017) can assist in the development of early-stage rifts by thermally and compositionally altering the lithosphere and consequently reducing its thickness and strength.

O'Donnell et al. (2016) calculated yield strength envelopes to estimate the strength of the lithosphere in nonmagmatic regions of the East African Rift System (EARS) and showed that extensional stresses in excess of 280 MPa would be needed to rift the East African lithosphere. A range of much lower extensional tectonic stresses have been estimated for East Africa (10–22 MPa, Stamps et al., 2014; 35 MPa, O'Donnell et al., 2016; 125 MPa, Craig et al., 2011), stresses that are clearly insufficient to initiate the rupture of >100 km thick, strong lithosphere. Therefore, magma-assisted rifting has been often invoked to explain rifting in East Africa, at least where Cenozoic volcanism is present (e.g., Ebinger & Sleep, 1998; Kendall et al., 2005).

The Malawi rift, situated near the southeastern end of the EARS (Figure 1), is a weakly extended continental rift (<15%; Ebinger et al., 1993) developed within Proterozoic mobile belts, and there is no evidence for volcanism within the rift itself. The Cenozoic Rungwe Volcanic Province (RVP), however, lies at the northern end of the rift, and weakening of the rifted lithosphere may have occurred if alteration of the lithosphere linked to the RVP volcanism is present to the south beneath the rift (Figure 1).

To illuminate crustal and upper mantle structure for investigating the process of early-stage rifting, the SEGMeNT (Study of Extension and maGmatism in Malawi aNd Tanzania) project obtained a suite of data sets, including active- and passive-source seismic, Global Positioning System, magnetotelluric, and geochemical in and around the northern Malawi rift (Shillington et al., 2016; Figure 1). In this paper, we utilize teleseismic earthquake data from the SEGMeNT project, as well as teleseismic data from previous networks in the study area, to investigate upper mantle structure beneath the northern Malawi rift and RVP to determine if there is seismic evidence for thermal and/or compositional alteration of the upper mantle that may have weakened the lithosphere and thus helped to promote rifting.

2. Background

The study area is located at the southeastern end of the Western rift, one arm of the EARS (Figure 1). The EARS is a divergent plate boundary over 4,000 km long, stretching from the Afar triple junction in the north to Mozambique in the southeast, and to Botswana in the southwest. The rift system south of Ethiopia comprises at least three branches, the Eastern, Western, and Southwestern rifts, which have mainly developed in Proterozoic mobile belts surrounding Archean cratons.

The study area includes the RVP and the Precambrian terranes that underlay the RVP and surround the northern portion of the Malawi rift (Figure 1a). The Malawi rift extends for ~800 km from the RVP in the north to the Urema Graben in the south. The majority of the rift is occupied by the ~40–60-km-wide Lake Malawi (Nyasa) and consists of several half-grabens bounded by long, large offset border faults (e.g., Ebinger et al., 1989; Specht & Rosendahl, 1989) and filled with up to 7 km of Paleozoic-Recent sedimentary strata (McCartney & Scholz, 2016). Rifting in parts of the Western rift may have initiated as early as 26 Ma (Roberts et al., 2012), and volcanism in the RVP initiated by ca. 17–18 Ma (Mesko et al., 2014; Rasskazov et al., 2003). The RVP lies within a complex accommodation zone between the Rukwa, Malawi, and Usangu rifts and includes three stratovolcanoes that have experienced Plinian and basaltic eruptions in the past 10 Ka (Ebinger et al., 1989; Fontijn, Delvaux, et al., 2010; Fontijn, Ernst, et al., 2010; Fontijn et al., 2012). The most common lavas within the RVP are basalts, trachytes, and phonolites (e.g., Fontijn, Delvaux, et al., 2010; Fontijn, Ernst, et al., 2010).

The Precambrian tectonic framework of the study region includes the Archean Tanzania Craton, just to the north of the RVP, the Bangweulu block, which lies to the southwest of the rift, and several Proterozoic mobile (orogenic) belts beneath and surrounding the RVP and Malawi rift (Figure 1). Based on geochemical analysis of sediments along the margins of the Bangweulu block, Andersen and Unrug (1984) argue that it is a Paleoproterozoic terrane. However, citing whole-rock geochemistry and isotopic data, DeWaele et al. (2006) contend that the Bangweulu block is an Archean craton, as originally proposed by Drysdall et al. (1972). The 1.92- to 1.83-Ga Usagaran Belt consists predominantly of granitoids and orthogneisses that were derived from reworking and recycling of the Tanzania Craton, while the Ubendian Belt consists mostly of granulite and amphibolite facies gneisses and metasedimentary rocks that formed during two orogenic

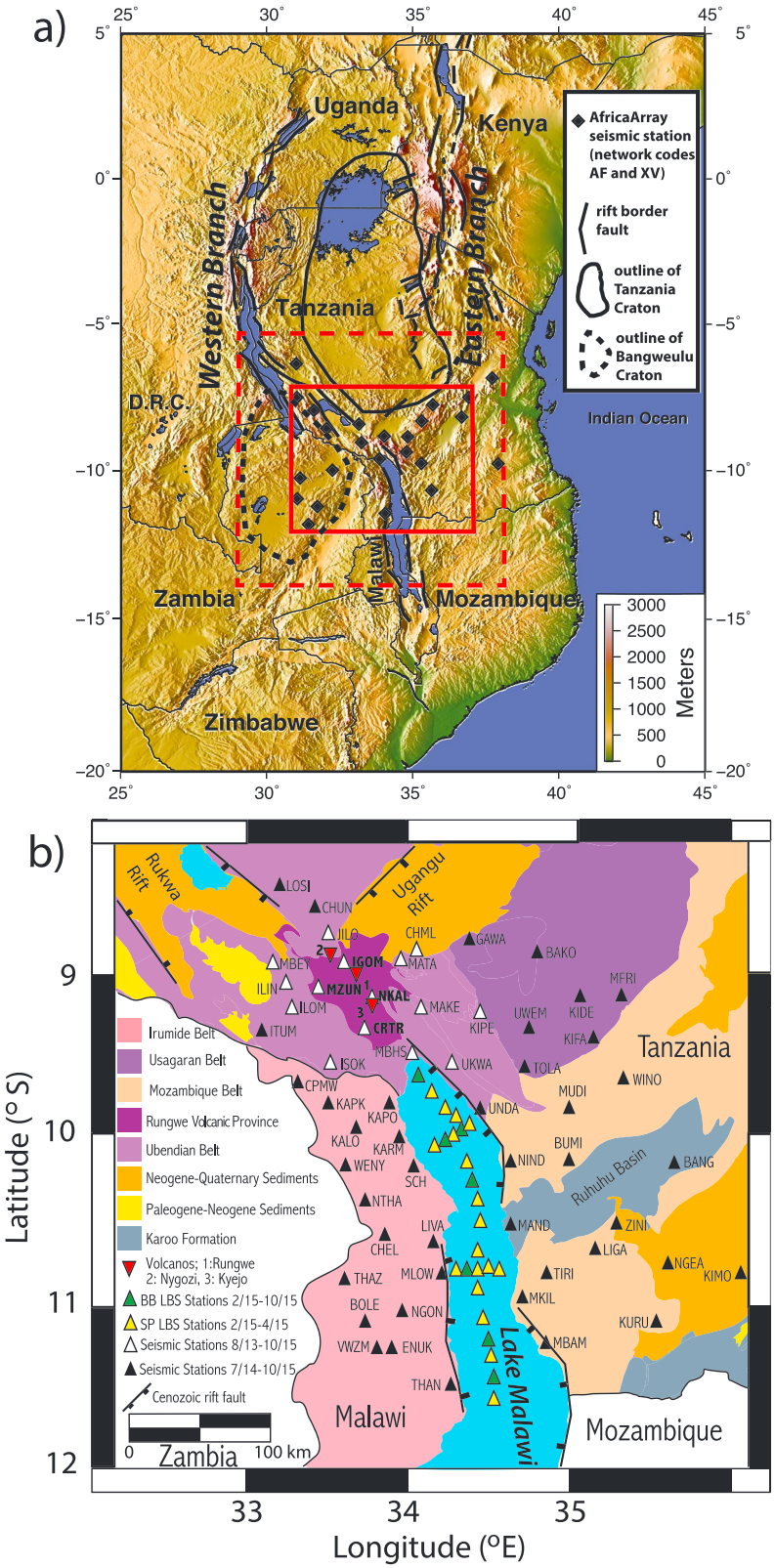


Figure 1. (a) Topographic map of eastern Africa showing the study area location. The red dashed line shows the outline of the model area and the solid red line shows the outline of the area in Figures 4 and 5. Craton boundaries shows the exposed margin of the cratons. (b) Geologic map of the area where Study of Extension and maGmatism in Malawi aNd Tanzania stations are located. Geological terrane boundaries are from Le Gall et al. (2004) and Pinna et al. (2004).

events between 2.03 and 1.86 Ga (Cahen et al., 1984; DeWaele et al., 2009; Lenoir et al., 1994; Schlüter & Hampton, 1997). The Irumide Belt consists of reworked Archean and Paleoproterozoic crust overlain by ~2-Ga rhyolites and sediments (Begg et al., 2009). During the Irumide orogeny ~1 Ga, the crust was strongly deformed by isoclinal folding and thrusting, resulting in crustal thickening with some addition of juvenile crust (DeWaele et al., 2006). The Mozambique Belt consists of gneisses and granulites and formed from multiple collision events between 1200 and 450 Ma (Cahen et al., 1984; Fritz et al., 2013).

2.1. Previous Seismic Imaging Studies

Previous seismic imaging studies of upper mantle beneath the Malawi rift and surrounding region have been restricted to a few regional-scale investigations (Adams et al., 2012; Mulibo & Nyblade, 2013a; O'Donnell et al., 2013, 2016), which imaged a ~100 to 200-km-wide low-velocity anomaly centered under the RVP. In the surface wave models of Adams et al. (2012) and O'Donnell et al. (2013), which have better depth resolution than the body wave tomography model of Mulibo and Nyblade (2013a), the low-velocity anomaly under the RVP extends to a depth of ~140–150 km, indicating that it is primarily a lithospheric scale feature. O'Donnell et al. (2013) attribute the anomaly to a ~200-K thermal perturbation of the lithospheric mantle and also possibly to the presence of partial melt. Body wave tomography models from Mulibo and Nyblade (2013a; Figure 2) and the surface wave tomography models of Adams et al. (2012) and O'Donnell et al. (2013) show fast craton-like upper mantle structure in northeastern Zambia in the vicinity of the Bangweulu Craton. O'Donnell et al. (2013) estimated the lithospheric thickness of the craton to be 150–200 km.

Limited resolution beneath the northern Malawi rift in these regional-scale studies leaves open the question of whether or not thermally perturbed upper mantle beneath the RVP extends to the south beneath the northern Malawi rift. Higher-resolution surface wave phase velocities from SEGMeNT suggest that low velocities extend southward from the RVP into the northern rift, but the anomaly is not as strong as that observed beneath the RVP (Accardo, Gaherty, et al., 2017). The Mulibo and Nyblade (2013a) body wave models (*P* and *S* waves) suggest that the low-velocity anomaly beneath the RVP may extend to the southeast under the rift (Figure 2) and also that the anomaly under the RVP may connect to the much larger upper mantle anomaly to the west, which Mulibo and Nyblade (2013a, 2013b) attributed to the African superplume (Figure 2).

In an interpretation of new shear wave splitting measurements in the study area, Tepp et al. (2018) found S-to-N along-axis variations in the fast polarization directions from a regional NE direction possibly associated with movement of African lithosphere with respect to a no-net rotation reference frame and enhanced by flow of the superplume mantle (Bagley & Nyblade, 2013). Tepp et al. (2018) argue that the shift from NE oriented fast polarization directions highly oblique to rift structure, to rift parallel from the RVP northward could indicate stagnation point flow around the thick lithosphere of the Bangweulu Craton and to the northwest beneath thinner lithosphere of the Ubendian Belt and Rukwa-Tanganyika rift zone.

3. Data and Modeling

Data used for this study were recorded between August 2013 and October 2015 by the SEGMeNT project (Shillington et al., 2016) seismic network (Figure 1). The network consisted of 57 broadband seismometers deployed across a 320 × 340-km region around northern Lake Malawi (YQ network code; https://doi.org/10.7914/SN/YQ_2013; Figure 1). Each station was equipped with a broadband seismometer (Guralp CMG3T, Streckeisen STS-2 or Nanometrics 120-s Trillium), a Reftek or Quanterra datalogger, and a Global Positioning System clock. Data were recorded continuously at 50 or 100 samples per second. During the first phase of deployment in August 2013, 14 stations were installed in and around the RVP (Figure 1). During the second phase of the deployment in August 2014, 43 additional stations were deployed, including 17 in Malawi and 26 in Tanzania. The station spacing in the network varied from 20 to 50 km. All stations recorded data continuously through late October 2015.

In addition to the land stations, the SEGMeNT network included 26 lake bottom seismometers (LBS) in Lake Malawi. Six of the LBS were broadband seismic stations operated from March 2015 to October 2015. Twenty short-period seismic stations operated from February 2015 to April 2015 (Figure 1). The broadband LBS stations were equipped with a broadband three-component Trillium 240 seismometer, as well as a differential pressure gauge. The short-period LBS stations were equipped with a three-component geophone and a hydrophone (Shillington et al., 2016).

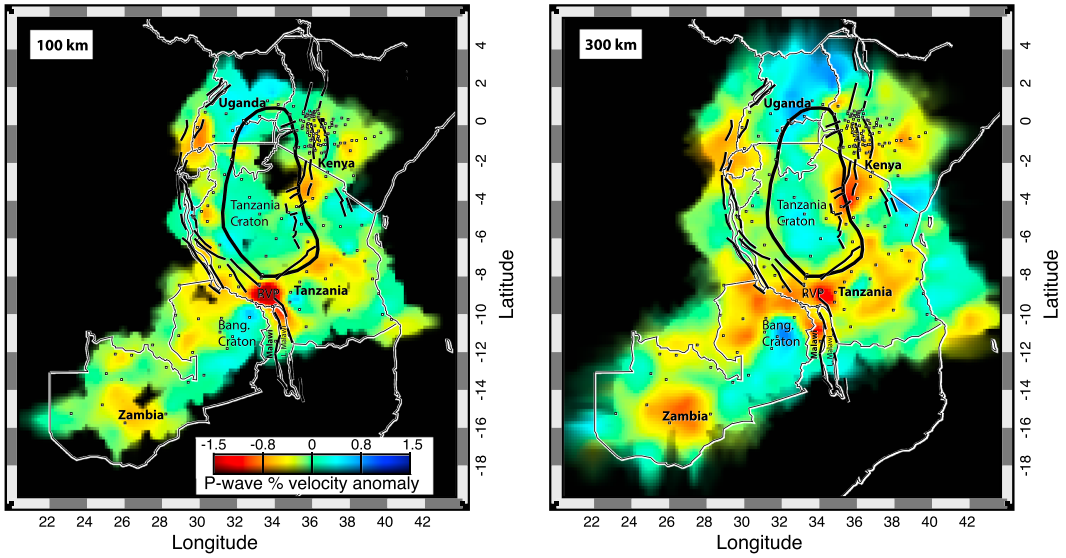


Figure 2. *P* wave tomography depth slices at 100-km (left) and 300-km (right) depths from Mulibo and Nyblade (2013a). Areas with hit counts <3 are shaded black. Bang. = Bangweulu Craton; RVP = Rungwe Volcanic Province. Bold black lines show major rift faults and outline of the Tanzania Craton. Small squares show seismic station locations.

Data from the SEGMeNT stations have been supplemented with data from the 2009–2011 AfricaArray deployment of broadband seismic stations in southern Tanzania and northern Zambia (network code ZP; https://doi.org/10.7914/SN/ZP_2007) and the permanent AfricaArray station in Mbeya, Tanzania (station MBEY; Figure 1). There are five overlapping stations between these networks. Four of the SEGMeNT stations (BAKO, CHML, MAKA, and CHIM) were collocated with stations deployed in 2009–2010 as part of the ZP network. The fifth overlapping station is the permanent AfricaArray station in Mbeya, Tanzania (station MBEY). The AfricaArray stations, when combined with the SEGMeNT stations, create a wider aperture network, enabling the imaging of mantle structure more broadly surrounding the RVP and northern Malawi rift. Additional station information is provided in Grijalva (2017).

Data used for this study come from teleseismic earthquakes with mb $\geq$ 5.5 in the 30° to 90° distance range of each station. *P* waves from 158 earthquakes and *S* waves from 130 earthquakes were recorded by the SEGMeNT stations and were supplemented by *P* wave and *S* wave arrival time picks from events recorded on the AfricaArray network (Figure 1). To remove high and low frequency energy prior to picking, a zero-phase bandpass filter with corner frequencies of 0.5 and 2 Hz for *P* waves and 0.04 to 0.2 Hz for *S* waves was applied to the data. The short-period LBS data were too noisy to pick *S* wave arrivals, limiting the *S* wave data set to travel times from just the land stations and the broadband LBS. Combined, data from all the stations resulted in a data set containing 12,412 *P* wave arrival times and 5,593 *S* wave arrival times. Lists of events used in the *P* and *S* wave tomography models can be found in Grijalva (2017). Figure 3 shows the event distribution for *P* and *S* waves, illustrating good azimuthal coverage.

To determine the relative arrival times, the multichannel cross correlation method of VanDecar and Crosson (1990), with arrival times from a minimum of five stations, was used for each event. Data windows of 3 s for *P* and 12 s for *S* waves surrounding the initial manually picked phase arrival were used for the cross-correlations (VanDecar & Crosson, 1990). All pairs of windowed traces for a given event were cross-correlated and relative arrival-times, Δtij, between pairs of stations *i,j* were obtained (VanDecar & Crosson, 1990). The relative arrival-times for the stations were then obtained by a least squares minimization of the residual for all station pairs (VanDecar & Crosson, 1990).

Before inverting the relative arrival time residuals for a three-dimensional velocity model, the residuals at the overlapping stations were compared as a function of back azimuth and distance to see if there were any systematic offsets in the residuals between the SEGMeNT and older data sets. No systematic differences were found (see example for station MBEY in supporting information Figure S4).

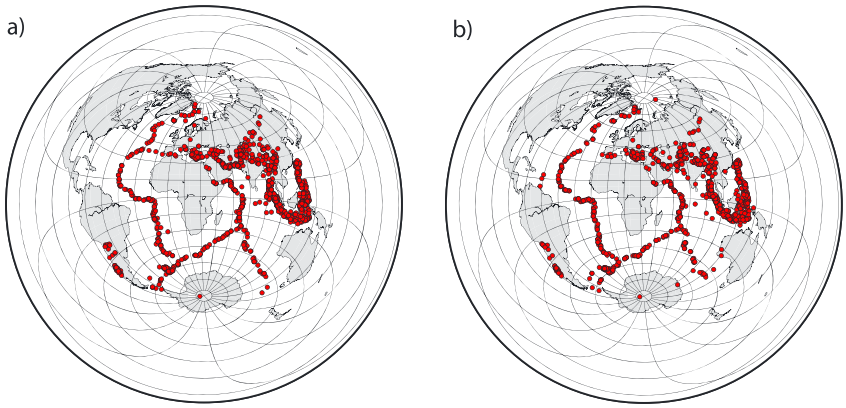


Figure 3. Teleseismic events used in this study. (a) *P* wave event locations. (b) *S* wave event locations.

VanDecar's (1991) method, which employs a least squares inversion, was used to invert the relative arrival time residuals for a three-dimensional velocity model. The model of the study region extends from 5 to 14°S to 29 to 38°E, and from the surface to 700 km depth. In this method, slowness is parameterized using splines under tension constrained at a series of regular knots. The grid encompassing the study region has 24 radial knots, 37 in the latitude, and 37 in the longitude, for a total of 32,856 knots. The grid's tightest spacing, 0.25° horizontally and 25 km vertically, is between 32 to 37°E and 8 to 12°S. The horizontal knot spacing increases to 1° outside this region. The radial nodes of the grid are spaced 25 km apart between 0- and 200-km depths, and 33 km between 200- and 700-km depths. The IASP91 global Earth model was used as a starting model for the inversion (Kennett & Engdahl, 1991).

The inversion method simultaneously inverts for slowness perturbations, source terms, and station terms (VanDecar, 1991). The source terms account for heterogeneous structure outside the model domain and source mislocations. The station terms absorb travel time variations arising from shallow structure directly beneath stations where the tomographic resolution is limited because of a lack of crossing rays. The inversion is underdetermined, and therefore regularization parameters (smoothing and flattening) are used to obtain a model with the least amount of structure that fits the data. The flattening parameter controls the anomaly amplitudes while the smoothing parameter controls the sharpness of the anomaly boundaries. The effects of the parameters are explored using trade-off curves (see Figure S2). The final *P* wave model, determined by using a smoothing of 120,000 and flattening of 5,000, accounts for ~94% of the *P* wave root-mean-square initial misfit (see Figure S1). The final *S* wave model, using identical smoothing and flattening parameters, accounts for ~89% of the *S* wave root-mean-square initial misfit (see Figure S2).

The station terms for both the *P* and *S* wave models are ~0.5–1.0 s on average (see Figures S3 and S4). Within the lake basin, the station terms are somewhat larger and can be explained by the presence of several kilometers of sediments in the rift basin. A similar range of station term values have been reported by others in East Africa using the VanDecar inversion method (Mulibo & Nyblade, 2013a; Park & Nyblade, 2006; Ritsema et al., 1998).

4. Model Results and Resolution

In the *P* wave model, the most prominent feature is a roughly circular low-velocity anomaly (low-velocity zone, LVZ) of δVp = ~−1.5–2.0% that is largely confined to the region underlying the RVP (Figure 4). The LVZ spans ~100–200 km horizontally and extends from 50 to ~250 km depth (Figure 4). The LVZ also extends to the southeast of the RVP beneath the center and northeastern side of the northern Malawi rift in the ~50- to 150-km depth interval (Figure 4). However, the amplitude (~1%) is smaller than the amplitude of the LVZ centered beneath the RVP. At about −10.5°, this anomaly shifts to the southwest under the central basin (Figure 1) and over to the western side of the rift. The anomaly widens further at depths ≥~200 km and extends to the north under northwestern Malawi, wrapping around a fast anomaly found at all depths in northeastern Zambia that correlates spatially with the location of the northeastern portion of the Bangweulu Craton.

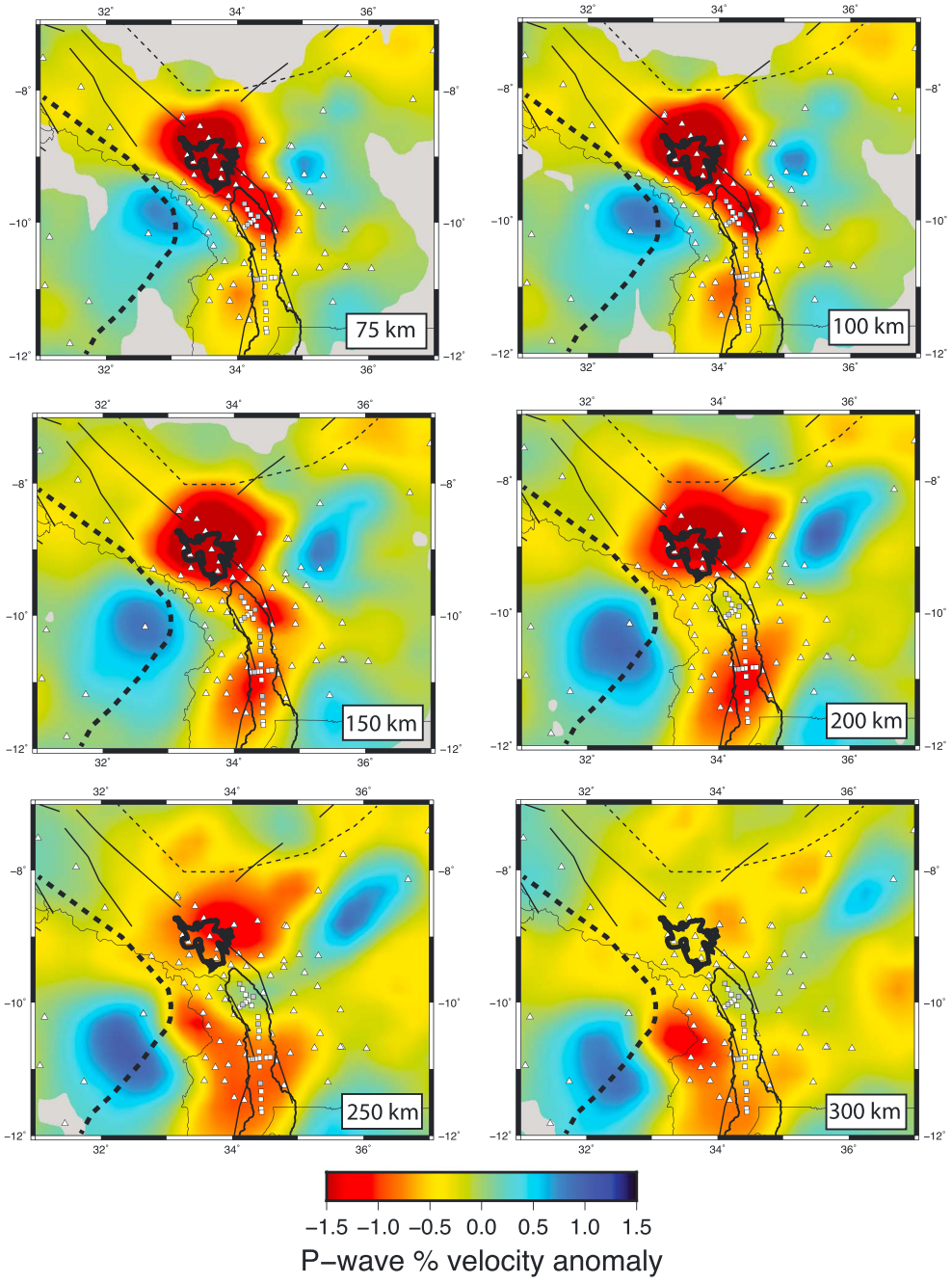


Figure 4. Depth slices through the *P* wave model. Seismic stations on land are shown with white triangles. Broadband lake bottom seismometers are shown with gray squares and short-period lake bottom seismometers with white squares. The outline of the Rungwe Volcanic Province is shown with a bold black line, and political boundaries are shown with a thin black line. The boundary of the Tanzania Craton (thin dashed line) and Bangweulu Craton (thick dashed line) and major rift faults are the same as in Figure 1a. This figure is available in colour online at wileyonlinelibrary.com/journal/ggge

The *S* wave model is similar to the *P* wave model. A prominent LVZ of $\delta Vs = \sim -2$–3% is found beneath the RVP at depths between 50 and ~300 km (Figure 5). As in the *P* wave model, a LVZ can be seen continuing from the RVP to the southeast underneath the center and northeastern side of the Malawi rift in the 50- to 150-km depth interval (Figure 5). A broader anomaly centered at about −11° is located beneath the central basin and the western side of the rift.

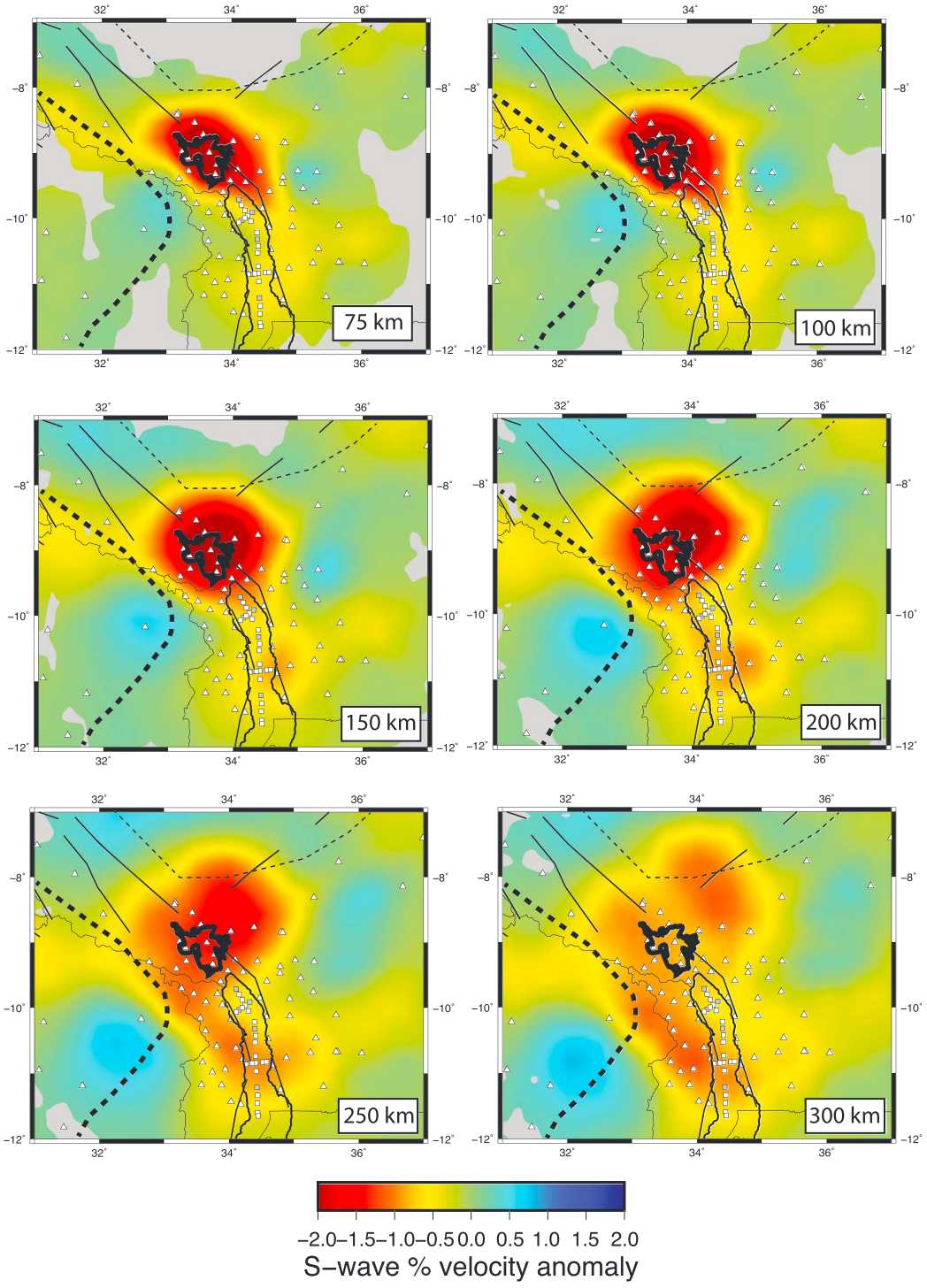


Figure 5. Depth slices through the *S* wave model. Seismic stations on land are shown with white triangles. Broadband lake bottom seismometers are shown with gray squares and short-period lake bottom seismometers with white squares. The outline of the Rungwe Volcanic Province is shown with a bold black line, and political boundaries are shown with a thin black line. The boundary of the Tanzania Craton (thin dashed line) and Bangweulu Craton (thick dashed line) and major rift faults are the same as in Figure 1a.

To evaluate model resolution, standard checkerboard tests composed of alternating positive and negative spherical (±5%) velocity anomalies were performed. Synthetic travel time data for the input models were generated using the actual ray paths, and 0.04-s random noise was added to the synthetic travel times for

the *P* wave data and 0.05 s for the *S* wave data. The synthetic travel times were inverted for velocity structure using the same model parameterization and inversion regularization as used in the inversion with the observed data.

The *P* wave checkerboard models consisting of 100-km-diameter Gaussian tapered spheres with peak amplitudes of ±5% are fairly well imaged, illustrating that structures on the order of 100 km wide can be resolved (Figure 6). The *S* wave model checkerboard results show checkers that are resolved spatially at the same level as for the *P* wave model, but with diminished amplitudes (Figure 6), indicating that the *P* wave model has better overall resolution than the *S* wave model. This result is expected given the travel time data set used for the *P* model is twice as large as the data set used for the *S* model. The results of checkerboard tests consisting of 50-km diameter checkers indicate very limited resolution at spatial scales of ~50 km for both the *P* and *S* wave models (Grijalva, 2017). Vertical slices through the 100-km wide recovered checkers indicates limited vertical resolution, with ≥100 km of vertical smearing (Figure 6).

5. Discussion

To summarize, the main features of the *P* and *S* wave models are (1) a LVZ with δVp = ~−1.5–2.0% and δVs = ~−2–3% centered beneath the RVP, (2) a lower-amplitude LVZ (δVp = ~−1.0–1.3% and δVs = ~−0.7–1%) to the southeast of the RVP beneath the center and northeastern side of the northern Malawi rift, (3) a shift of the lower-amplitude anomaly at ~−10° to −11° to the west beneath the central basin and to the western side of the rift, (4) a fast anomaly at all depths beneath the Bangweulu Craton in northeastern Zambia. The LVZ widens further at depths >~150–200 km and extends to the north beneath northwestern Malawi, wrapping around the fast anomaly beneath the Bangweulu Craton. These features are more clearly seen in the *P* wave model than the *S* wave model because the *P* wave model has better resolution.

The velocity reductions in our models could be caused by several factors, such as temperature, composition, grain size, partial melt, and anisotropy (e.g., Faul & Jackson, 2005; Goes et al., 2000; Jackson & Faul, 2010; Karato & Karki, 2001; Sobolev et al., 1996; Yamauchi & Takei, 2016). For interpreting the anomalies, we use the results of Goes et al. (2000), in which the sensitivities of *Vp* and *Vs* to temperature, anelasticity, and composition in the ~50- to 250-km depth range are reported in units of % velocity anomaly/100 K. In this study, several representative upper mantle compositions are considered (e.g., average continental garnet/spinel lherzolite, Archean subcontinental lithospheric mantle, Proterozoic subcontinental lithospheric mantle, tectonic subcontinental lithospheric mantle) that can be used to estimate upper bounds on lateral changes in seismic velocities caused by compositional variations.

Using the relationships in Goes et al. (2000), we interpret the anomalies taking into consideration the amplitude recovery in our resolution tests. Because of the regularization used in the inversion, the velocity anomaly magnitudes are underestimated. In the 100- to 200-km depth interval, the checkerboard resolution tests show amplitude recovery in the RVP area of ~30% for *Vp* and ~25% for *Vs*. Scaling up the imaged *Vp* and *Vs* anomaly magnitudes (−1.5–2.0% and −2–3%, respectively) yields RVP anomaly magnitudes of *Vp* = ~−5–6.5% and *Vs* = ~−8–12%. According to Goes et al. (2000), the %*Vp* and %*Vs* velocity variations that would be expected in transitioning from a baseline average continental garnet lherzolite to subcontinental lithosphere below tectonic regions are <0.05% *Vp* and <−0.6% *Vs* for depths of 50 to 200 km. This compositional signature increases slightly if transitioning from a baseline average continental garnet lherzolite to Archean subcontinental lithospheric mantle, but it never exceeds 1% for either *Vp* or *Vs* (Goes et al., 2000). Therefore, placing an upper limit of 1% on compositional variations leaves RVP anomalies of at least *Vp* = ~−4–5.5% and *Vs* = ~−7–11% that must be explained by some combination of temperature, melt, or other fluids.

Regarding temperature, Goes et al. (2000) predict that a 100-K increase in temperature is associated with a decrease in *Vp* of 0.5–2% and in *Vs* of 0.7–4.5%. Using this, the up-scaled RVP anomalies (*Vp* = ~−4–5.5%, Vs = ~−7–11%) would translate to temperature anomalies of 200–1100 and 155–1570 K, respectively. The combined lower limit (155–200 K) serves as a low temperature bound for the RVP anomaly, which is consistent with the temperature anomaly of ~200 K predicted by O'Donnell et al. (2013) using an *S* wave model derived from surface wave tomography. The upper limits are implausibly high unless the presence of melt or other fluids is invoked. However, estimating the amount of melt is difficult because it depends not only on the amount of melt, but also on the melt geometry. Nevertheless, following Goes et al. (2000), who

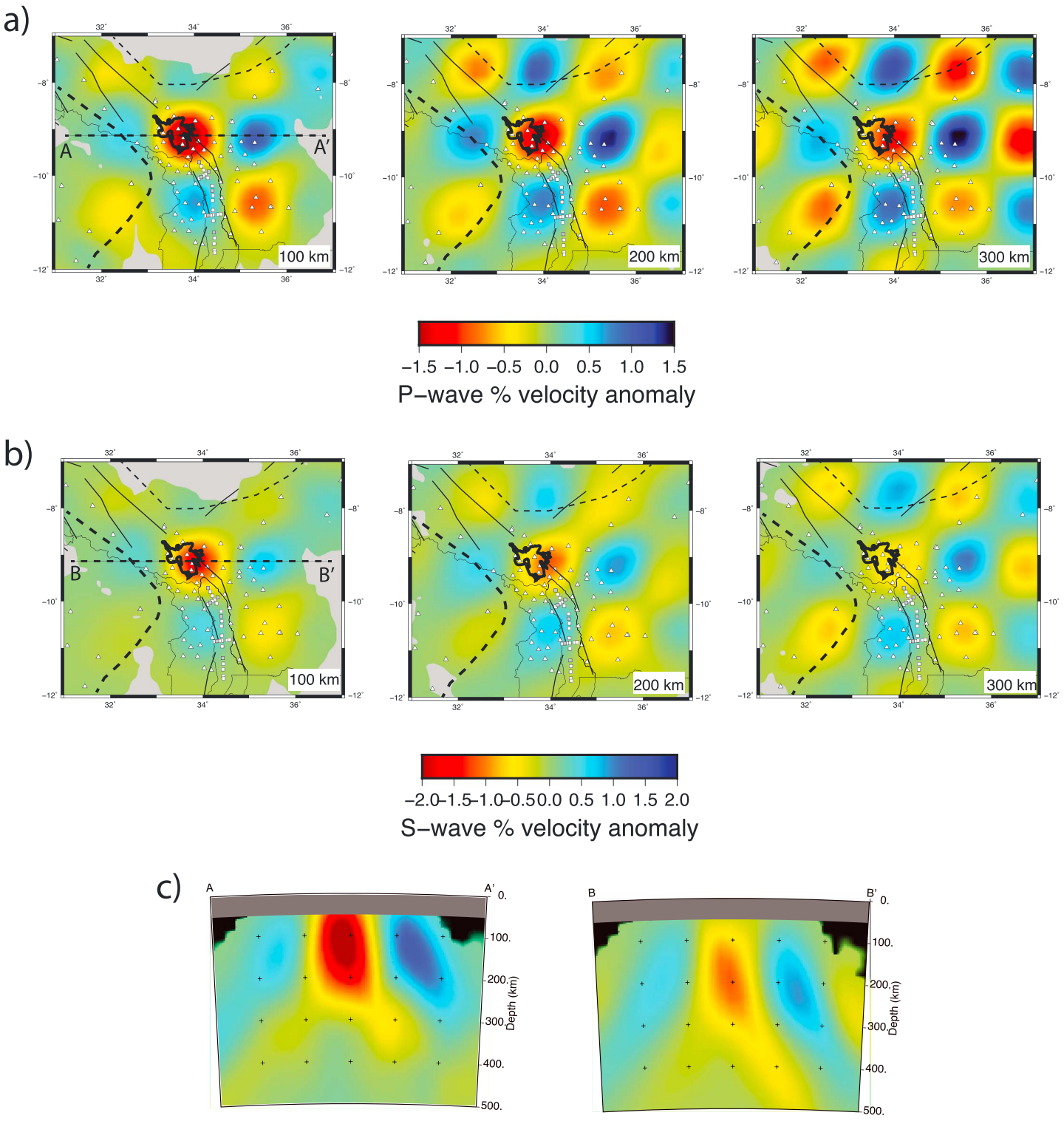


Figure 6. Checkerboard resolution tests for 100-km-wide checkers. (a) Recovered checkers at depths of 100, 200, and 300 km for the *P* wave model. (b) Recovered checkers at depths of 100, 200, and 300 km for the *S* wave model. (c) Recovered checkers for vertical slices A–A′ in *P* model and B–B′ in *S* model. Seismic stations on land are shown with white triangles. Broadband lake bottom seismometers are shown with gray squares and short-period lake bottom seismometers with white squares. The outline of the Rungwe Volcanic Province is shown with a bold black line, and political boundaries are shown with a thin black line. The boundary of the Tanzania Craton (thin dashed line) and Bangweulu Craton (thick dashed line) and major rift faults are the same as in Figure 1a.

show that aspect ratios between 1 and 0.01 predict a 0.5–3.5% decrease of *Vp* per % melt, and 0.7–8.5% decrease of *Vs* per % melt, the presence of melt could account for a significant amount of the RVP *Vp* and *Vs* anomalies. Applying the same lines of reasoning to the *Vp* and *Vs* anomalies to the south of the RVP beneath the center and northeastern side of the northern Malawi rift indicate a lower limit on the thermal anomaly there of ~50–100 K.

The lower bound on the RVP temperature anomaly of 155–200 K is consistent with an alternative approach estimating the temperature anomaly using the shear wave velocity temperature derivative of 8×10^{-4} km/s/K reported by Faul and Jackson (2005), which is based on assuming an average grain size of 10 mm and temperature of 1300° C for the upper mantle. In this case, the *S* wave velocity anomaly of ~−2–3% yields a temperature anomaly of ~200 K, and a much larger temperature anomaly if the upscaled *Vs* anomaly is used. Faul and Jackson (2005) predict that the effect of changing grain size by a factor of 10 (i.e., from 1 mm to 1 cm) corresponds to about a 0.5–1% change in velocity, and therefore, even if the 10-mm average grain size assumption is incorrect for the RVP, the presence of melt or other fluids is still required to explain the upscaled *Vs* anomaly.

Invoking melt or other fluids within the upper mantle, in addition to elevated temperatures, to explain the RVP is supported by other evidence. Petrological data from the RVP indicate a hydrated, CO_2-rich magma source zone, there is evidence for extensive He in the shallow crust beneath the RVP, and at least one volcano is actively degassing large volumes of CO_2 (Barry et al., 2013; Furman, 1995; Mesko et al., 2014). In addition, Rooney et al. (2012), based on geochemical analyses of 53 primitive magmas throughout East Africa, concluded that regionally extensive low-velocity anomalies beneath the EARS could not be attributed entirely to elevated mantle temperatures. They suggested that CO_2-assisted melt production in the African superplume could be one factor contributing to the low seismic velocities beneath the EARS. The *Vp* and *Vs* anomalies in our models therefore likely reflect a combination of locally elevated temperature, small volume melt production, and local volatile concentrations.

Because the *P* wave model is better resolved than the *S* wave model, we base the geodynamic interpretation of our results primarily on the *P* wave model. As mentioned above, the LVZ appears to wrap around the fast lithosphere of the Bangweulu Craton, indicating that the location of the anomaly is strongly influenced by the presence of the cratonic lithosphere. To explain shear wave splitting patterns in the study area, Tepp et al. (2018) proposed that warm mantle material from the larger African superplume structure to the west and south enhances the shear induced by NE directed African plate motion (see Figure 10 in Tepp et al., 2018). As the enhanced flow encounters the edge of the thick Bangweulu Craton lithosphere and rises beneath thinner orogenic belt lithosphere, a small upward-directed counterflow is generated, potentially explaining the melt generation at the craton-orogenic belt intersection.

Figure 7 illustrates that our results are consistent with an interpretation invoking warm mantle flowing beneath and around the Bangweulu Craton lithosphere. The boundary between the LVZ and the fast structure of the Bangweulu Craton in profiles B–B′, C–C′, and D–D′ in Figure 7 is fairly sharp, as would be expected for warm, perhaps compositionally distinct, mantle material upwelling along the edge of thick, cold cratonic lithosphere. Because of the vertical smearing of structures common to body wave tomography, imaging the warm mantle flow beneath the Bangweulu Craton is a challenge (i.e., the fast structure of the cratonic lithosphere smears downward to >300-km depth). Nonetheless, profiles B–B′, C–C′, and D–D′ in Figure 7 suggest low-velocity mantle beneath the fast structure of the Bangweulu Craton lithosphere. We thus argue for an interpretation, similar to Tepp et al. (2018), invoking the flow of warm, superplume mantle giving rise to the LVZ seen on our model beneath both the RVP and the northern Malawi rift. This interpretation is also consistent with the larger scale tomographic models of Mulibo and Nyblade (2013a; Figure 2), which show in the 100- to 300-km depth interval a LVZ wrapping around the eastern, northern, and western sides of the Bangweulu Craton, as well as with high $^3He/^4He$ values from the RVP indicating melt contributions from a deeply sourced upwelling (Barry et al., 2013; Halldorsson et al., 2014; Hilton et al., 2011).

The presence of an LVZ extending under the RVP and much of the northern Malawi rift indicates that the rifted lithosphere has been thermally perturbed and that the location of the thermal perturbation is influenced to a large degree by the presence of the Bangweulu Craton. Although there is no volcanism within the Malawi rift to suggest thermal weakening of the lithosphere, it is apparent from our results that the lithosphere beneath the rift has been thermally perturbed. We are not able to place any constraints on the timing

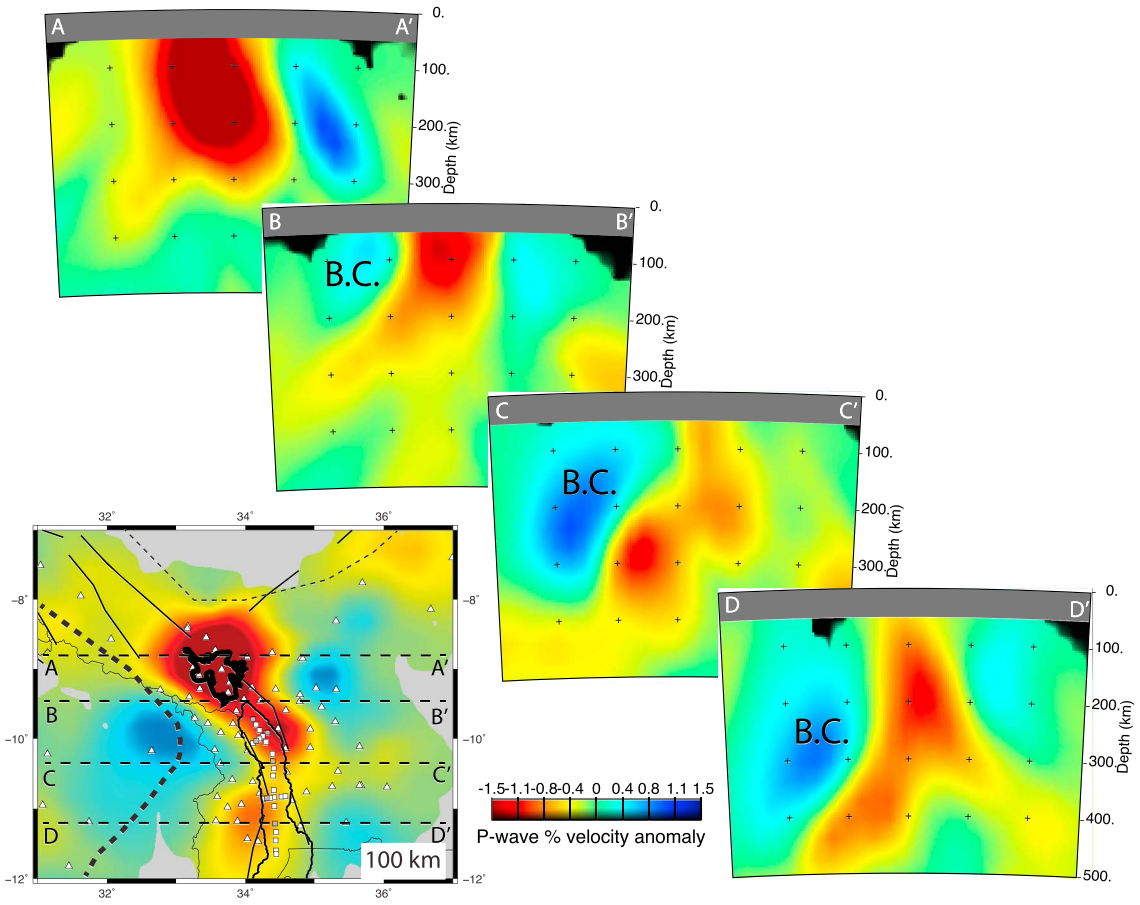


Figure 7. Vertical slices through *P* wave model showing the fast structure of the B.C. and the slow structure under the northern Malawi rift to the east of the craton (B–B′, C–C′, and D–D′) and under the Rungwe Volcanic Province (A-A′). The locations of the vertical slices are shown on the map (100-km depth slice from Figure 4) in lower left.

of the thermal perturbation, but given there is evidence for rift volcanism in the region starting as early as 26 Ma (Roberts et al., 2012), and that volcanism in the RVP began ca. 17–18 Ma (Mesko et al., 2014; Rasskazov et al., 2003), whereas much of the rift morphology developed in the past 10 Ma (Ebinger et al., 1989; McCartney & Scholz, 2016; Specht & Rosendahl, 1989), thermal and magmatic (metasomatism, local heating) weakening of the lithosphere could have begun prior to the onset of rifting, as noted by Mesko et al. (2014).

An additional question is why the amplitude of the RVP LVZ is so large compared to the amplitude of the LVZ under the northern Malawi rift, and why is it located north of the rift? One possibility for the larger anomaly amplitude, as discussed already, is the presence of larger amounts of melt or other fluids beneath the RVP, as would be expected given the volcanic history of the RVP. Long-lived (18 Myr) magma intrusion into the RVP lithosphere may have resulted in local heating, enhanced thinning, and more decompression melting than beneath the stretched lithosphere to the NW and SSE, at least in part explaining the localized nature of the pronounced LVZ under the RVP. Another possibility, suggested by Tepp et al. (2018), is that preexisting lithospheric thickness variations between orogenic belts and cratons (Tanzania, Bangweulu) causes divergence of the flow into several streams (stagnation point flow). And a third possibility is that the amplitude and location of the RVP anomaly could arise in part from warm mantle pooling on the underside of locally thinned lithosphere. The RVP is located beneath the intersection of Mesozoic and Cenozoic rift zones (e.g., Ebinger et al., 1989). There is some evidence for rift volcanism in the region starting as early as 26 Ma (Roberts et al., 2012) and older sediments beneath the northernmost part of Lake Malawi likely deposited during previous rifting episodes (Accardo, Shillington, et al., 2017). If lithospheric extension in the RVP area during the very initial stages of Cenozoic rifting was greater than in the rift branches to the northwest

(Rukwa rift), northeast (Usangu rift), and south (Malawi rift; Figure 1), and if that extension was superimposed on already thinned lithosphere from Mesozoic rifting, then a small region of thinned lithosphere may have existed where upwelling material could have ponded. Such warm, ponded material could contribute to the strong RVP velocity anomaly, as well as to the development of the RVP itself. The Mesozoic through Cenozoic rift history of the region is not well understood, particularly because much of the region is covered by the Rungwe volcanics, and therefore quantifying the amount of lithospheric thinning caused by Mesozoic and/or Cenozoic extension is difficult. Nevertheless, given the RVP's location at the intersection of three previously and presently active rifts, the lithosphere there likely has experienced more extensive thinning compared to the regions surrounding it.

6. Summary and Conclusions

New *P* and *S* wave tomographic models have been developed for the northern Malawi rift and adjacent RVP. The main features of the models are (1) a LVZ with $\delta Vp = \sim -1.5–2.0\%$ and $\delta Vs = \sim -2–3\%$ centered beneath the RVP, (2) a lower-amplitude LVZ ($\delta Vp = \sim -1.0–1.3\%$ and $\delta Vs = \sim -0.7–1\%$) to the southeast of the RVP beneath the center and northeastern side of the northern Malawi rift, (3) a shift of the lower-amplitude anomaly at $\sim -10°$ to $-11°$ to the west beneath the central basin and to the western side of the rift, and (4) a fast anomaly at all depths beneath the Bangweulu Craton in northeastern Zambia. The LVZ widens further at depths $>\sim$150–200 km and extends to the north beneath northwestern Malawi, wrapping around the fast anomaly beneath the Bangweulu Craton. The *P* and *S* wave anomalies under the RVP indicated a temperature anomaly of at least 155–200 K, while the anomalies beneath the center and northeastern side of the northern Malawi rift indicate a lower limit on the thermal anomaly there of ~50–100 K.

We attribute the LVZ beneath both the RVP and the northern Malawi rift to the flow of warm, superplume mantle, moving from the southwest to the northeast, upwelling beneath and around the Bangweulu Craton lithosphere. In this interpretation, as the flow encounters the edge of the thick Bangweulu Craton lithosphere, it rises beneath thinner orogenic belt lithosphere to the east, creating the low-velocity anomalies that we image. The boundary between the LVZ and the fast structure of the Bangweulu Craton in our models is fairly sharp, which is consistent with warm, perhaps compositionally distinct, mantle material upwelling along the edge of thick, cold cratonic lithosphere. This interpretation is also consistent with high $^{3}He/^{4}He$ values from the RVP, which indicate melt contributions from a deeply sourced upwelling.

The presence of an LVZ extending under the RVP and much of the northern Malawi rift strongly indicates that the rifted lithosphere has been thermally perturbed. Although we are not able to place constraints on the timing of the thermal perturbation, given that volcanism in the RVP began earlier than much of the rift faulting, thermal and magmatic (metasomatism, local heating) weakening of the lithosphere could have begun prior to the onset of rifting.

One possibility for the larger anomaly amplitude localized beneath the RVP is the presence of larger amounts of melt or other fluids beneath the RVP, as would be expected given the volcanic history of the RVP. Long-lived (18 Myr) magma intrusion into the RVP lithosphere may have resulted in local heating, enhanced thinning, and more decompression melting than beneath the stretched lithosphere to the NW and SSE, at least in part explaining the pronounced LVZ. It is also possible that the amplitude and location of the RVP LVZ may arise, at least in part, from warm mantle pooling on the underside of locally thinned lithosphere. The RVP is located beneath the intersection of Mesozoic and Cenozoic rift zones, and if lithospheric extension in the RVP area during the very initial stages of rifting was greater than in neighboring rift branches, then a small region of thinned lithosphere may have formed where upwelling material could have ponded. Such warm, ponded material could contribute to the strong RVP velocity anomaly, as well as to the development of the RVP itself.

Acknowledgments
Funding for this program was provided by the National Science Foundation (NSF) through Awards EAR-1109293, 1109302, 1109512, 1110882, and 1110921 and by Lamont-Doherty Earth Observatory of Columbia University. Acquisition of this data set would not have been possible without the support from communities in the study area, national and regional governmental entities in Malawi and Tanzania, and the IRIS PASSCAL program. Seismic data used for this project (https://doi.org/10.7914/SN/YQ_2013) are openly available from the IRIS Data Management Center. We thank Tyrone Rooney and an anonymous reviewer for comments that greatly improved this paper.

References

Accardo, N., Gaherty, J., Shillington, D., Ebinger, C., Nyblade, A., Mbogoni, G., et al. (2017). Surface-wave imaging of the weakly-extended Malawi rift from ambient-noise and teleseismic Rayleigh waves from onshore and lake-bottom seismometers. *Geophysical Journal International*, *209*(3), 1892–1905. https://doi.org/10.1093/gji/ggx133

Accardo, N. J., D. J. Shillington, J.B. Gaherty, C. A. Scholz, C. Ebinger, A. Nyblade, and et al. (2017). Evidence for strong controls from preexisting structure on border fault development and basin evolution in the Malawi rift from 3D lacustrine refraction data. American Geophysical Union, Fall Meeting Abstracts.

Adams, A., Nyblade, A., & Weeraratne, D. (2012). Upper mantle shear wave velocity structure beneath the East African plateau: Evidence for a deep, plateau-wide low velocity anomaly. *Geophysical Journal International*, *189*(1), 123–142. https://doi.org/10.1111/j.1365-246X.2012.05373.x

Andersen, L. S., & Unrug, R. (1984). Geodynamic evolution of the Bangweulu Block, northern Zambia. *Precambrian Research*, *25*(1–3), 187–212 . https://doi.org/10.1016/0301-9268(84)90032-9

Bagley, B., & Nyblade, A. A. (2013). Seismic anisotropy in Eastern Africa, mantle flow, and the African superplume. *Geophysical Research Letters*, *40*, 1500–1505. https://doi.org/10.1002/grl.50315

Barry, P. H., Hilton, D. R., Fischer, T. P., De Moor, J. M., Mangasini, F., & Ramirez, C. (2013). Helium and carbon isotope systematics of cold "mazuku" CO2 vents and hydrothermal gases and fluids from Rungwe Volcanic Province, southern Tanzania. *Chemical Geology*, *339*, 141–156. https://doi.org/10.1016/j.chemgeo.2012.07.003

Bastow, I. D., & Keir, D. (2011). The protracted development of the continent-ocean transition in Afar. *Nature Geoscience*, *4*, 248–250. https://doi.org/10.1038/ngeo1095

Begg, G., Griffin, W., Natapov, L., O'Reilly, S., Grand, S., O'Neill, C., & et al. (2009). *The lithospheric architecture of Africa: Seismic tomography, mantle petrology, and tectonic evolution*. Boulder: Geological Society of America, Inc.

Bialas, R., Buck, R., & Qin, R. (2010). How much magma is required to rift a continent? *Earth and Planetary Science Letters*, *292*(1-2), 68–78. https://doi.org/10.1016/j.epsl.2010.01.021

Bott, M. H. P. (1991). Ridge push and associated plate interior stress in normal and hot spot regions. *Tectonophysics*, *200*(1-3), 17–32. https://doi.org/10.1016/0040-1951(91)90003-B

Buck, W. R. (2004). Consequences of asthenospheric variability on continental rifting. In G. D. Karner, B. Taylor, N. W. Driscoll, & D. L. Kohlstedt (Eds.), *Rheology and deformation of the lithosphere at continental margins*, (Vol. 62, pp. 1–30). New York: Columbia Univ. Press. https://doi.org/10.7312/karn12738-002

Buck, W. R. (2006). The role of magma in the development of the Afro-Arabian rift system. In G. Yirgu, C. J. Ebinger, & P. K. H. Maguire (Eds.), *The Afar volcanic province within the East African rift system*. *Geological Society of London*, 43–54.

Cahen, L., Snelling, N. J., Delhal, J., & Vail, J. R. (1984). *The Geochronology and Evolution of Africa* (512 pp.). Oxford: Oxford University Press.

Craig, T. J., Jackson, J. A., Priestley, K., & McKenzie, D. (2011). Earthquake distribution patterns in Africa: Their relationship to variations in lithospheric and geological structure, and their rheological implications. *Geophysical Journal International*, *185*(1), 403–434. https://doi.org/10.1111/j.1365-246X.2011.04950.x

DeWaele, B., Fitzsimons, I. C. W., Wingate, M. T. D., Tembo, F., Mapani, B., & Belousova, E. A. (2009). The geochronological framework of the Irumide Belt: A prolonged crustal history along the margin of the Bangweulu Craton. *American Journal of Science*, *309*(2), 132–187. https://doi.org/10.2475/02.2009.03

DeWaele, B., Liegeois, J. P., Nemchin, A. A., & Tembo, F. (2006). Isotopic and geochemical evidence of proterozoic episodic crustal reworking within the Irumide Belt of south-central Africa, the southern metacratonic boundary of an Archaean Bangweulu Craton. *Precambrian Research*, *148*(3–4), 225–256. https://doi.org/10.1016/j.precamres.2006.05.006

Drysdall, A. R., Johnson, R. L., Moore, T. A., & Thieme, J. G. (1972). Outline of the geology of Zambia. *Geologie en Mijnbouw*, *51*, 265–276.

Ebinger, C., Deino, A., Drake, R., & Tesha, A. (1989). Chronology of volcanism and rift basin propagation: Rungwe volcanic province, East Africa. *Journal of Geophysical Research*, *94*(B11), 15,785–15,803. https://doi.org/10.1029/JB094iB11p15785

Ebinger, C. J., Deino, A. L., Tesha, A. L., Becker, T., & Ring, U. (1993). Tectonic controls on rift basin morphology: Evolution of the Northern Malawi (Nyasa) rift. *Journal of Geophysical Research*, *98*(B10), 17,821–17,836. https://doi.org/10.1029/93JB01392

Ebinger, C. J., & Sleep, N. H. (1998). Cenozoic magmatism throughout East Africa resulting from impact of a single plume. *Nature*, *395*(6704), 788–791. https://doi.org/10.1038/27417

Faul, U., & Jackson, I. (2005). The seismological signature of temperature and grain size variations in the upper mantle. *Earth and Planetary Science Letters*, *234*(1-2), 119–134. https://doi.org/10.1016/j.epsl.2005.02.008

Foley, S., & Fischer, T. (2017). An essential role for continental rifts and lithosphere in the deep carbon cycle. *Nature Geoscience*, *10*(12), 897–902. https://doi.org/10.1038/s41561-017-0002-7

Fontijn, K., Delvaux, D., Ernst, G., Kervyn, M., Mbede, E., & Jacobs, P. (2010). Tectonic control over active volcanism at a range of scales: Case of the Rungwe Volcanic Province, SW Tanzania; and hazard implications. *Journal of African Earth Sciences*, *58*(5), 764–777. https://doi.org/10.1016/j.jafrearsci.2009.11.011

Fontijn, K., Ernst, G., Elburg, M., Williamson, D., Abdallah, E., Kwelwa, S., & et al. (2010). Holocene explosive eruptions in the Rungwe Volcanic Province, Tanzania. *Journal of Volcanology and Geothermal Research*, *196*(1-2), 91–110. https://doi.org/10.1016/j.jvolgeores.2010.07.021

Fontijn, K., Williamson, D., Mbede, E., & Ernst, G. G. J. (2012). The Rungwe Volcanic Province, Tanzania—A volcanological review. *Journal of African Earth Sciences*, *63*, 12–31. https://doi.org/10.1016/j.jafrearsci.2011.11.005

Fritz, H., Abdelsalam, M., Ali, K. A., Bingen, B., Collins, A. S., Fowler, A. R., et al. (2013). Orogen styles in the East African Orogen: A review of the Neoproterozoic to Cambrian tectonic evolution. *Journal of African Earth Sciences*, *86*, 65–106. https://doi.org/10.1016/j.jafrearsci.2013.06.004

Furman, T. (1995). Melting of metasomatized subcontinental lithosphere: Undersaturated mafic lavas from Rungwe, Tanzania. *Contributions to Mineralogy and Petrology*, *122*(1–2), 97–115. https://doi.org/10.1007/s004100050115

Goes, S., Govers, R., & Vacher, P. (2000). Shallow mantle temperatures under Europe from P and S wave tomography. *Journal of Geophysical Research*, *105*, 11,153–11,169.

Grijalva, A., (2017), P and S body wave tomography of the northern Lake Malawi rift basin and Rungwe volcanic province, (M.S. thesis, pp. 141). Pennsylvania State Univ.

Halldorsson, S. A., Hilton, D. R., Scarsi, P., Abede, T., & Hopp, J. (2014). A common mantle plume source beneath the entire East African rift System revealed by coupled helium-neon systematics. *Geophysical Research Letters*, *41*, 2304–2311. https://doi.org/10.1002/2014GL059424

Hilton, D. R., Halldorsson, S. A., Barry, P. H., Fischer, T. P., de Moor, J. M., Ramirez, C. J., et al. (2011). Helium isotopes at Rungwe Volcanic Province, Tanzania, and the origin of East African Plateaux. *Geophysical Research Letters*, *38*, L21304. https://doi.org/10.1029/2011gl049589

Jackson, I., & Faul, U. H. (2010). Grainsize-sensitive viscoelastic relaxation in olivine: Towards a robust laboratory-based model for seismological application. *Physics of the Earth and Planetary Interiors*, *183*(1-2), 151–163. https://doi.org/10.1016/j.pepi.2010.09.005

Kampunzu, A. B., & Mohr, P. (1991). Magmatic evolution and petrogenesis in the East African rift system. In *Magmatism in extensional structural settings*, (pp. 85–136). Berlin Heidelberg: Springer. https://doi.org/10.1007/978-3-642-73966-8_5

Karato, S., & Karki, B. B. (2001). Origin of lateral variation of seismic wave velocities and density in the deep mantle. *Journal of Geophysical Research*, *106*(B10), 21,771–21,783. https://doi.org/10.1029/2001JB000214

Kendall, J.-M., Stuart, G. W., Ebinger, C. J., Bastow, I. D., & Keir, D. (2005). Magma-assisted rifting in Ethiopia. *Nature*, *433*(7022), 146–148. https://doi.org/10.1038/nature03161

Kennett, B., & Engdahl, E. (1991). Traveltimes for global earthquake location and phase identification. *Geophysical Journal International*, *122*, 429–465.

Le Gall, B., Gernigon, L., Rolet, J., Ebinger, C., Gloaguen, R., Nilsen, O., et al. (2004). Neogene–Holocene rift propagation in central Tanzania: Morphostructural and aeromagnetic evidence from the Kilombero area. *Geological Society of America Bulletin*, *116*(3), 490–510. https://doi.org/10.1130/B25202.1

Lenoir, J. L., Liégeois, J. P., Theunissen, K., & Klerkx, J. (1994). The Palaeoproterozoic Ubendian shear belt in Tanzania: Geochronology and structure. *Journal of African Earth Sciences*, *19*(3), 169–184. https://doi.org/10.1016/0899-5362(94)90059-0

McCartney, T., & Scholz, C. A. (2016). A 1.3 million year record of synchronous faulting in the hanging wall and border fault of a half-graben in the Malawi (Nyasa) Rift. *Journal of Structural Geology*, *91*, 114–129. https://doi.org/10.1016/j.jsg.2016.08.012

Mesko, G. T., Class, C., Maqway, M. D., Boniface, N., Manya, S., & Hemming, S. R. (2014). The timing of early magmatism and extension in the Southern East African Rift: Tracking geochemical source variability with $^{40}Ar/^{39}Ar$ geochronology at the Rungwe Volcanic Province, SW Tanzania. AGU Fall Meeting Abstracts (Vol. 1, p. 4730).

Morgan, W. J. (1971). Convection plumes in the lower mantle. *Nature*, *230*(5288), 42–43. https://doi.org/10.1038/230042a0

Mulibo, G., & Nyblade, A. (2013b). Mantle transition zone thinning beneath eastern Africa: Evidence for a whole-mantle superplume structure. *Geophysical Research Letters*, *40*, 3562–3566. https://doi.org/10.1002/grl.50694

Mulibo, G. D., & Nyblade, A. A. (2013a). The P and S wave velocity structure of the mantle beneath eastern Africa and the African superplume anomaly. *Geochemistry, Geophysics, Geosystems*, *14*, 2696–2715. https://doi.org/10.1002/ggge.20150

O'Donnell, J. P., Adams, A., Nyblade, A., Mulibo, G., & Tugume, F. (2013). The uppermost mantle shear wave velocity structure of eastern Africa from Rayleigh wave tomography: Constraints on rift evolution. *Geophysical Journal International*, *194*(2), 961–978. https://doi.org/10.1093/gji/ggt135

O'Donnell, J. P., Selway, K., Nyblade, A., Brazier, R., El Tahir, N., & Durrheim, R. (2016). Thick lithosphere, deep crustal earthquakes and no melt: A triple challenge to understanding extension in the western branch of the East African Rift. *Geophysical Journal International*, *204*(2), 985–998. https://doi.org/10.1093/gji/ggv492

Park, Y., & Nyblade, A. A. (2006). P-wave tomography reveals a westward dipping low velocity zone beneath the Kenya rift. *Geophysical Research Letters*, *33*, L07311. https://doi.org/10.1029/2005GL025605

Pinna, P., Muhongo, S., Le Goff, E., Mcharo, B.A., Deschamps, Y., Milesi, J.P., et al. (2004) Geology and mineral map of Tanzania (scale 1:2,000,000). Geol. Sur. Fra. Orleans.

Rasskazov, S. V., Logachev, N. A., Ivanov, A. V., Boven, A. A., Maslovskaya, M. N., Saranina, E. V., et al. (2003). A magmatic episode in the western rift of East Africa (19–17 Ma). *Geologiya i Geofizika*, *44*(4), 317–324.

Ritsema, J., Nyblade, A. A., Owens, T., Langston, C., & VanDecar, J. (1998). Upper mantle seismic velocity structure beneath Tanzania, East Africa: Implications for the stability of cratonic lithosphere. *Journal of Geophysical Research*, *103*(B9), 21,201–21,213. https://doi.org/10.1029/98JB01274

Roberts, E. M., Stevens, N. J., O'Connor, P. M., Dirks, P. H. G. M., Gottfried, M. D., Clyde, W. C., et al. (2012). Initiation of the western branch of the East African Rift coeval with the eastern branch. *Nature Geoscience*, *5*(4), 289–294. https://doi.org/10.1038/ngeo1432

Rooney, T. O., Herzberg, C., & Bastow, I. D. (2012). Elevated mantle temperature beneath East Africa. *Geology*, *40*(1), 27–30. https://doi.org/10.1130/G32382.1

Rooney, T. O., Nelson, W. R., Ayalew, D., Hanan, B., Yirgu, G., & Kappelman, J. (2017). Melting the lithosphere: Metasomes as a source for mantle-derived magmas. *Earth and Planetary Science Letters*, *461*, 105–118. https://doi.org/10.1016/j.epsl.2016.12.010

Rooney, T. O., Nelson, W. R., Dosso, L., Furman, T., & Hanan, B. (2014). The role of continental lithosphere metasomes in the production of HIMU-like magmatism on the northeast African and Arabian plates. *Geology*, *42*(5), 419–422. https://doi.org/10.1130/G35216.1

Rosenthal, A., Foley, S. F., Pearson, D. G., Nowell, G. M., & Tappe, S. (2009). Petrogenesis of strongly alkaline primitive volcanic rocks at the propagating tip of the western branch of the East African Rift. *Earth and Planetary Science Letters*, *284*(1-2), 236–248. https://doi.org/10.1016/j.epsl.2009.04.036

Schlüter, T., & Hampton, C. (1997). *Geology of East Africa*. Berlin: Borntraeger.

Sengör, A. M. C., & Burke, K. (1978). Relative timing of rifting and volcanism on Earth and its tectonic implications. *Geophysical Research Letters*, *5*(6), 419–421. https://doi.org/10.1029/GL005i006p00419

Shillington, D., Gaherty, J., Ebinger, C., Scholz, C., Scholz, A., Selway, K., et al. (2016). Acquisition of a unique onshore/offshore geophysical and geochemical dataset in the northern Malawi (Nyasa) rift. *Seismological Research Letters*, *87*(6), 1–11.

Sobolev, S. V., Zeyen, H., Stoll, G., Werling, F., Altherr, R., & Fuchs, K. (1996). Upper mantle temperatures from teleseismic tomography of French Massif Central including effects of composition, mineral reactions, anharmonicity, anelasticity and partial melt. *Earth and Planetary Science Letters*, *139*(1-2), 147–163. https://doi.org/10.1016/0012-821X(95)00238-8

Specht, T. D., & Rosendahl, B. R. (1989). Architecture of the Lake Malawi Rift, East Africa. *Journal of African Earth Sciences*, *8*(2-4), 355–382. https://doi.org/10.1016/S0899-5362(89)80032-6

Stamps, D. S., Flesch, L. M., Calais, E., & Ghosh, A. (2014). Current kinematics and dynamics of Africa and the East African Rift System. *Journal of Geophysical Research: Solid Earth*, *119*, 5161–5186. https://doi.org/10.1002/2013JB010717

Tepp, G., Ebinger, C. J., Zal, H., Gallacher, R., Accardo, N., Shillington, D. J., et al. (2018). Seismic anisotropy of the upper mantle below the Western rift, East Africa. *Journal of Geophysical Research: Solid Earth*, *123*(7), 5644–5660. https://doi.org/10.1029/2017JB015409

VanDecar, J., & Crosson, R. (1990). Determination of teleseismic relative phase arrival times using multi-channel cross-correlation and least squares. *Bulletin of Seismological Society of America*, *80*, 150–169.

VanDecar, J. C. (1991). Upper mantle structure of the Cascadia subduction zone from nonlinear teleseismic travel time inversion, (Ph. D. thesis). Seattle, WA: Univ. of Washington.

White, R., & McKenzie, D. (1989). Magmatism at rift zones: The generation of volcanic continental margins and flood basalts. *Journal of Geophysical Research*, *94*(B6), 7685–7729. https://doi.org/10.1029/JB094iB06p07685

Yamauchi, H., & Takei, Y. (2016). Polycrystal anelasticity at near-solidus temperatures. *Journal of Geophysical Research: Solid Earth*, *121*, 7790–7820. https://doi.org/10.1002/2016JB013316